

Intrinsic piezoelectricity of PZT

Desheng Fu^{1,2,3*}, Seiji Sogen² and Hisao Suzuki⁴

¹*Department of Electronics and Materials Science,
Faculty of Engineering,
Shizuoka University, 3-5-1 Johoku,
Chuo-ku, Hamamatsu 432-8561, Japan.*

²*Department of Engineering,
Graduate School of Integrated Science and Technology,
Shizuoka University, 3-5-1 Johoku,
Chuo-ku, Hamamatsu 432-8561, Japan.*

³*Department of Optoelectronics and Nanostructure Science,
Graduate School of Science and Technology,
Shizuoka University, 3-5-1 Johoku,
Chuo-ku, Hamamatsu 432-8011, Japan.*

⁴ *Research Institute of Electronics,
Shizuoka University, 3-5-1 Johoku,
Chuo-ku, Hamamatsu 432-8011, Japan.*

email:fu.tokusho@shizuoka.ac.jp

Abstract

An unresolved issue in the commonly used $\text{Pb}(\text{Zr}_{1-x}\text{Ti}_x)\text{O}_3$ (PZT) ceramics is understanding the intrinsic piezoelectric behaviors of its crystal around the morphotropic phase boundary (MPB). Here, we demonstrate an approach to grow c -axis oriented tetragonal PZT around MPB on stainless steel SUS430, allowing us to estimate the intrinsic piezoelectric and ferroelectric properties of PZT along its polar axis. The piezoelectric coefficient d_{33} and spontaneous polarization P_s were found to be 46.4 ± 4.4 pm/V, 88.7 ± 4.6 $\mu\text{C}/\text{cm}^2$, respectively, for $x = 0.47$ close to MPB. These values align well with the predicted values of $d_{33} = 50 \sim 55$ pC/N and $P_s = 79$ $\mu\text{C}/\text{cm}^2$ at room temperature from the first-principles-derived approach. The obtained d_{33} is 4 times smaller than that of its ceramics, indicating that the large piezoelectric response in the PZT ceramics around MPB is primarily driven by extrinsic effects rather than intrinsic ones. In the technical application of PZT films, achieving a substantial piezoelectric response requires careful consideration of these extrinsic effects.

Keywords: PZT, morphotropic phase boundary (MPB), piezoelectric, ceramics, single crystal, oriented film, piezoelectric coefficient d_{33}

I. INTRODUCTION

$\text{Pb}(\text{Zr}_{1-x}\text{Ti}_x)\text{O}_3$ (PZT) is an alloy of antiferroelectric PbZrO_3 and ferroelectric PbTiO_3 . It exhibits a nearly vertical morphotropic phase boundary (MPB) in the vicinity of $x = 0.47 - 0.50$, separating the ferroelectric rhombohedral and tetragonal phases. PZT ceramics display an exceptionally large piezoelectric response in the vicinity of the MPB.¹⁻³ This characteristic has established PZT ceramics as the primary workhorse in the realm of piezoelectric devices, with widespread applications in various fields, including ultrasonic imaging in medicine, sensors in automobiles, and atomic positioning in science.⁴

Beyond its evident technological significance, PZT holds fundamental importance. The MPB concept derived from PZT has frequently guided the design of new materials with significant physical property response. This has led to the successful discovery of high piezoelectric responses in ferroelectrics^{5,6} and large magnetic responses in ferromagnets stemming from the MPB.^{7,8} Clearly, comprehending the fundamental physics involved in MPB remains a critical concern in the fields of material sciences and condensed matter physics,⁹⁻²⁸ which may pave the way for designing new functional materials with excellent physical properties.

Understanding the intrinsic piezoelectric behaviors of PZT single crystals near the MPB have been a longstanding challenge. Since its discovery seven decades ago,²⁹ substantial and continuous efforts have been dedicated to growing high-quality single crystals of PZT.³⁰⁻³⁴ However, the unavailability of PZT single crystals with high quality has hindered the determination of their intrinsic piezoelectric properties near the MPB. Consequently, theoretical approaches have been employed to address this issue. A semi-empirical simulation work on the basis of phenomenological Landau Devonshire theory predicts that a PZT single crystal would have a d_{33} value of 520 pm/V in the rhombohedral phase and 325 pm/V in the tetragonal phase along the polar axis near MPB.³⁵ The large d_{33} observed in PZT ceramics is attributed to be the response of a single crystal. In contrast, the first-principles calculations have found that the d_{33} values of a tetragonal PZT single crystal with $x = 0.5$ is 3 times less than the experimental value observed for ceramics at low temperatures.^{36,37} Furthermore, first-principles-derived approach has been developed to study the finite-temperature properties of PZT around MPB, and the d_{33} is predicted to be $50 \sim 55$ pC/N for a tetragonal single crystal of PZT($x=0.5$) at room temperature,³⁸ which is approximately 6 times smaller than the one derived from phenomenological Landau Devonshire theory. The theoretical results

derived from first-principles calculations and Landau theory calculations are fundamentally different. Therefore, even from a theoretical perspective, the intrinsic piezoelectric effects of PZT single crystal remain unclear.

It is clear that the intrinsic piezoelectric response of PZT near MPB ultimately still requires experimental confirmation. The key to addressing this issue lies in the investigation of the linear piezoelectric effect in PZT along its polar axis, which is solely caused by the lattice deformation induced by an electric field. In this communication, we present a method to grow polar-axis oriented PZT to identify the intrinsic piezoelectric response near MPB. The piezoelectric coefficient d_{33} and spontaneous polarization P_s were experimentally found to be 46.4 ± 4.6 pm/V, 71.4 ± 11.3 $\mu\text{C}/\text{cm}^2$, respectively, in PZT with $x = 0.47$ close to MPB. Our experimental results fully support the predictions based on the first-principles calculations by L. Bellaiche et. al.^{37,38} and indicate that the high piezoelectric response in PZT ceramics is primarily driven by the extrinsic effects rather than the intrinsic effects of lattice response.

II. EXPERIMENTAL

We utilized chemical solution deposition³⁹ to grow the tetragonal c -axis oriented PZT with $x = 0.47$, close to MPB. We have successfully developed an approach to grow the c -axis oriented PZT through using a stainless steel SUS430 substrate and a metallic LaNiO_3 (LNO) seed layer, as schematically shown in Fig.1. LNO possesses a pseudocubic perovskite structure with a lattice constant of $a = 3.838\text{\AA}$, comparable to that of PZT with a perovskite structure. Moreover, LNO exhibits the least surface energy for the (100)-plane growth, enabling full (100)-plane growth even on an amorphous substrate.⁴⁰ Therefore, the (100)-oriented LNO effectively serves as a seed layer to guide the growth of (100)- or (001)-oriented PZT with tetragonal structure on SUS430 substrate. We further used the significant difference in thermal expansion coefficient between SUS430 and PZT to achieve (001)-plane growth of tetragonal PZT, allowing us to apply a compressive thermal stress to PZT unit cell during cooling from the growth temperature. This compressive thermal stress greatly promotes the c -axis growth of tetragonal PZT as the crystal transitions from the cubic to tetragonal phase during cooling. A $0.24\text{-}\mu\text{m}$ -thick (100)-oriented LNO was grown at 700°C for 5 minutes in an oxygen atmosphere from the LNO precursor solution prepared

from $\text{La}(\text{NO}_3)_3$, $\text{Ni}(\text{CH}_3\text{COO})_2$, and solvents of 2-methoxyethanol and 2-aminoethanol. The detailed process for preparing LNO is illustrated in Fig.S1 of the supporting information and can also be found in the previous report.³⁹

To prevent the diffusion of Cr from SUS430 to PZT, which typically reduces the crystalline quality and physical properties of PZT, a 0.3- μm -thick SiO_2 buffer layer was placed between LNO and SUS430. The detailed process for preparing SiO_2 is shown in Fig.S2 of the supporting information. The SiO_2 precursor solution was prepared by dissolving $\text{Si}(\text{OC}_2\text{H}_5)_4$ in ethanol, followed by hydrolysis with water in the presence of hydrochloric acid as an acid catalyst. The purpose of the SiO_2 layer is to prevent chromium diffusion from the substrate, necessitating a dense structure. Using hydrochloric acid as a catalyst leads to the formation of precursor with linear or cross-linked molecular chain, enabling the creation of a dense film. The precursor solution was deposited on a SUS430 substrate by spin coating at 2500 rpm for 30 seconds. It was then dried at 150°C for 10 minutes, pre-annealed at 350°C for 10 minutes to eliminate organic matter, and finally fired at 700°C for 10 minutes in an oxygen atmosphere to form the SiO_2 layer. This process was repeated three times to achieve the desired film thickness of the SiO_2 layer.

PZT was subsequently grown on the LNO/ SiO_2 /SUS430 substrate at 650°C in an oxygen atmosphere using a precursor solution prepared from $\text{Pb}(\text{OCOCH}_3)_2 \cdot 3\text{H}_2\text{O}$, $\text{Zr}(\text{OC}_3\text{H}_7)_4$, $\text{Ti}(\text{OCH}(\text{CH}_3)_2)_4$, and absolute ethanol as solvent. The detailed process for preparing PZT films are shown in Fig.S3 of the supporting information. To produce high-quality PZT thin films, we developed the precursor solution using metal alkoxides, employing a partial hydrolysis approach for Zr- and Ti-alkoxides with a chemical modification using acetic acid and controlling water addition for hydrolysis. This process led to the creation of Zr-O-Ti chemical bonds in the precursor solution, paving the way for exceptionally high-quality PZT films. PZT was grown to a thickness of 0.3 ~ 1.2 μm , which is sufficient to disregard the impact of two-dimensional strain from the substrate on the overall physical properties of PZT.⁴¹

The crystal structure of the films was observed using a BRUKER AXS D8 ADVANCE X-ray diffractometer with Cu $k\alpha$ radiation. The surface of the films was examined using both field emission scanning electron microscopy (FE-SEM, JEOL JSM-7001F) and atomic force microscopy (AFM, SPI3800N, SII). Cross-sectional images of the film were obtained through transmission electron microscopy (TEM) using a JEM-2100F. The sample for TEM

measurement was prepared by focused ion beam (FIB) with a JEOL JIB 4500.

Toyof ferroelectric tester system (FCE-3) in conjunction with SII AFM was used to examine the polarization-switching and displacement behaviors of these *c*-axis oriented PZT films. The samples, grown on 1 cm \times 1 cm SUS430, were mounted on the AFM scanner using silver paste to firmly unite the scanner and SUS430 substrate, preventing the sample from bending. The measurements were conducted on capacitors with 60- μ m-diameter top Pt electrodes and conducting LNO bottom electrode at room temperature, at a frequency of 1 Hz. This low-frequency measurement allows for more complete switching of spontaneous polarization compared to the frequency of 1 kHz commonly reported in the literature.

III. RESULTS AND DISCUSSION

Figure 2 shows the X-ray diffraction patterns of the PZT samples with thickness from 0.3 \sim to 1.2 μ m. This result indicates that our approach successfully enabled the growth of *c*-axis (polar-axis) oriented PZT with a tetragonal structure on the SUS430 substrate. The lattice constant was determined to be 4.110 \AA from the (004) diffraction peak observed in the XRD patterns, which is independent of the thickness of the PZT film in the range from 0.3 \sim 1.2 μ m. This value aligns excellently with the *c*-axis lattice constant of its bulk counterpart, which exhibits tetragonal symmetry with $c=4.113\text{\AA}$ and $a=4.019\text{\AA}$ at room temperature.²⁹ The independence of the lattice constant with film thickness and the agreement of the lattice constant between the sample and its bulk further verify that the grown PZT lattice has been fully relaxed from substrate strain. Consequently, the overall physical properties of the sample can be regarded as those of the bulk material.

Figure 3 shows the surface and cross-sectional morphology of the *c*-axis oriented PZT film. From the cross-sectional view, it is evident that the growth mechanism of the PZT thin film is completely different from that of the LNO film. The LNO film appears to have experienced granular growth, whereas the PZT has grown in a columnar fashion. The average diameter of the columnar PZT is about 103 nm, with a variation of 41 nm when observed from the surface. Since the columnar interfaces are not visible in the cross-section, it can be inferred that these columnar PZT crystals are interconnected. The surface of the PZT film is relatively smooth, with an average roughness of 0.88 nm as observed by AFM, and the height variation is within a few nanometers. An interesting phenomenon observed on the surface

is that some areas in the SEM image appear darker while others are brighter, with both the bright and dark areas displaying uniform brightness. This FE-SEM observation was made without coating the surface with a metallic film. Since the brightness variation reflects the surface's charge state, it is reasonable to consider that the appearance of bright and dark areas is due to the emergence of 180-degree domains with opposite polarization directions. The observations from FE-SEM are consistent with the previously described X-ray results and the subsequent polarization hysteresis and piezoelectric measurement results.

Figure 4 illustrates typical results of the $D - E$ hysteresis loop, the switching current, and the electric-field-induced displacement for various applied bipolar or unipolar voltages using 600-nm thick PZT samples as an example. For the c -axis oriented PZT with tetragonal symmetry, only the 180-degree domain switching is anticipated when the sample is subjected to an electric field in the direction of spontaneous polarization. When the applied voltage exceeds the coercive field greatly, the switching current nearly drops to zero, and the electrical polarization reaches saturation. This indicates that the spontaneous polarization has been almost entirely switched to the field direction under such a high electric field in the c -axis oriented PZT sample. This is further corroborated by the displacement response of the sample obtained at the same time (Fig.4(c)). The c -axis oriented PZT sample exhibits the typical strain response behavior predicted for the single crystal, as shown in the inset of Fig.4(c).⁵⁰ A linear piezoelectric response has been observed in the sample when removing the applied voltage, indicating almost complete alignment of spontaneous polarization with the field direction. For the case of unipolar field measurements, the displacement was measured after poling the sample. Once again, we have observed the linear piezoelectric effects as anticipated from the lattice response in the unipolar field measurements. The above results clearly indicate that the spontaneous polarization in c -axis oriented PZT has been aligned with the field direction. Under this state, one can use a linear fitting to estimate the intrinsic piezoelectric coefficient d_{33} of PZT, in which the extrinsic effects such as the domain effects are essentially negligible.

Fig.5 summarizes the results of the $D - E$ hysteresis loop and the electric-field-induced displacement of the c -axis oriented PZT shown in Fig.2. All samples demonstrate similar polarization switching and displacement behaviors. We then use the linear change in displacement with the applied voltage to calculate the piezoelectric coefficient d_{33} of these c -axis oriented PZTs by linear fitting. All samples show similar results for the piezoelectric

coefficient, as depicted in Fig.6. The d_{33} was estimated to be 46.4 ± 4.4 pm/V from the statistical calculation of all the results obtained from both the bipolar and unipolar displacement measurements of all samples. Our experimental d_{33} aligns well with the first-principles prediction for PZT single crystal near MPB.³⁸ Using a first-principles-derived approach, Bellaiche et al. studied the finite-temperature behaviors of PZT near the MPB and demonstrated that the d_{33} of single-crystal PZT with $x = 0.5$ is around 50-55 pC/N at room temperature. However, our experimental d_{33} result disagrees with the prediction from the phenomenological Landau Devonshire theory by Du et al.,³⁵ who predicted a d_{33} value of 325 pm/V for the c -axis tetragonal PZT single crystal with $x = 0.5$, about 7 times larger than our value. This overestimated d_{33} is very likely caused by the accuracy of the Landau free-energy coefficients used in the calculation.⁴² Unlike first-principles calculations, which offer insights at the atomic scale, Landau phenomenology provides a macroscopic understanding through experimental fitting parameters and cannot capture microscopic details. Moreover, the fitting parameters used for free-energy calculations are obtained from ceramics and are different from those of single crystals, leading to an incorrect estimation of the piezoelectric coefficients of the PZT single crystal.

The first-principles-derived calculation by Bellaiche et al. also predicted a spontaneous polarization of $79 \mu\text{C}/\text{cm}^2$ for this PZT single crystal near the MPB.³⁸ This prediction aligns well with our experimental statistical result of $88.7 \pm 4.6 \mu\text{C}/\text{cm}^2$ as shown in Fig.6. In our analysis, we estimate the spontaneous polarization (P_S) from the $D - E$ hysteresis loop by assuming that electrical displacement density D is proportional to the electric field E when all spontaneous polarizations have been aligned along the field direction and make an extrapolation to obtain the spontaneous polarization P_S at zero field, as shown in Fig.4(a) and Fig.5.

Our d_{33} of PZT with $x = 0.47$ around MPB compares well with those reported for epitaxial PZT films with higher PbTiO_3 content and larger tetragonality c/a .⁴³⁻⁴⁵ The lattice distortion caused by an electric field has been shown to result in d_{33} values of 50 pm/V for the epitaxial 250-nm-thick PZT film with $x = 0.65$ and $c/a = 4.133\text{\AA}/3.989\text{\AA} = 1.036$,⁴³ 65 pm/V for the epitaxial 2- μm -thick PZT film with $x = 0.65$ and $c/a = 4.152\text{\AA}/3.991\text{\AA} = 1.040$,⁴⁵ and 45 pm/V for the epitaxial 35-nm-thick PZT film with $x = 0.8$ and $c/a = 4.25\text{\AA}/3.905\text{\AA} = 1.088$.⁴⁴ Our result and those reported values for epitaxial PZT are rather comparable to the d_{33} value of 83.7 pm/V reported for PT single crystal.⁴⁶ The above com-

parison is also summarized in Fig.7. All these experimental findings confirm the prediction derived from first-principles calculations that the piezoelectric coefficients of tetragonal PZT around MPB are rather comparable to those of the simple PbTiO_3 .^{36,37,47,48} For example, Bellaiche et al. predicted that the tetragonal PZT with $x = 0.5$ and PbTiO_3 would have e_{33} piezoelectric coefficients of 3.4 C/m^2 and 3.8 C/m^2 , respectively, and thus concluded that "alloying PbTiO_3 with PbZrO_3 does not provide any enhancement of piezoelectricity with respect to PT".³⁷ This conclusion derived from first-principles calculations is supported by our experimental result for PZT near MPB and those reported for PT single crystal and epitaxial PZT single-crystalline films with different PT concentrations.

In contrast, PZT ceramics exhibit different piezoelectric behaviors. In ceramics, the piezoelectric response is dependent on the PT concentration, and a maximum occurs around the MPB with $x = 0.48$.¹ PZT ceramics near the MPB with $x = 0.48$ show a d_{33} piezoelectric coefficient of 223 pm/V ,¹ which is 4~5 times larger than the 51 pm/V reported for PT ceramics⁴⁹ and our own measurements of the polar c -axis d_{33} of tetragonal PZT with an MPB composition of $x=0.47$.^{1,14} For a comparison, the ceramics values reported for PZT by Belincourt et al.¹ and for PT by Ikegami et al.⁴⁹ are also replotted in Fig.7.

The significant d_{33} piezoelectric coefficient observed in PZT ceramics near the MPB cannot be solely attributed to the intrinsic d_{33} piezoelectric effect of the single crystal. Instead, it is largely influenced by extrinsic effects. A key extrinsic factor is the movement of domain walls or domain switching within the PZT ceramics.^{17,24,25,27,28,50,51}

Near the MPB, PZT ceramics exhibit a complex domain structure due to the coexistence of tetragonal, rhombohedral, and monoclinic phases.¹⁴ This complexity is further accentuated by the presence of nano-domains, averaging around 10 nm in size.²⁶ The high density and mobility of these nano-domain walls contribute substantially to the overall piezoelectric response (d_{33}), introducing nonlinear contributions beyond the intrinsic lattice strain.

Additionally, the coexistence of tetragonal and rhombohedral phases, interconnected by the monoclinic phase near the MPB,¹⁴ facilitates interactions and local transformations between these phases under an applied electric field.^{19,21,23} This phase transformation mechanism allows the ceramics to accommodate larger strains, thereby enhancing the piezoelectric response.

In polycrystalline PZT ceramics, grain boundaries also play a critical role in influencing piezoelectric behavior. These boundaries can act as sites for stress concentration and fa-

facilitate additional strain mechanisms that are not present in single-crystal materials. Unlike free-standing single crystal, the grains in ceramics are mechanically constrained by their neighboring grains. This mechanical constraint results in significant elastic strain during non-180° domain switching. Such intergranular and intragranular strains^{15,16,24} can substantially enhance the piezoelectric response in PZT ceramics.

The significant d_{15} effects predicted in PZT from first-principles calculations seem to provide a plausible and reliable explanation for the large d_{33} piezoelectric effect in PZT ceramics near the MPB. Using the predicted d_{15} value of 580 pm/V, Bellaiche et al. successfully estimated a value of 163 pV/m for PZT ceramics with $x = 0.5$ near the MPB at room temperature,³⁸ which closely matches the reported value of 173 pm/V for PZT ceramics with $x = 0.5$.¹ The large shear piezoelectric coefficient d_{15} predicted for PZT crystal is consistent with the experimental results reported for ceramics, as shown in Fig. 7, which indicate a d_{15} of 494 pm/V for PZT ceramics near the MPB¹ but only 53 pm/V for PT ceramics.⁴⁹ However, further confirmation is needed for the single crystal.

IV. CONCLUSIONS

In summary, we have presented a straightforward method to uncover the intrinsic piezoelectric behaviors of PZT near the MPB along the polar axis. We found that PZT with $x = 0.47$ exhibits a d_{33} piezoelectric coefficient of 46.4 ± 4.4 pm/V and a spontaneous polarization of 88.7 ± 4.6 $\mu\text{C}/\text{cm}^2$ along the polar c -axis of the tetragonal structure. Our experimental results align well with predictions from first-principles-derived calculations but contradict with those from phenomenological calculations. Our findings indicate that the significant piezoelectric effect (d_{33}) observed in PZT ceramics near the MPB is primarily driven by extrinsic effects, rather than the crystal's intrinsic piezoelectric properties. These extrinsic effects include enhanced domain wall mobility, phase coexistence and transformation, and intergranular and intragranular strain effects. These mechanisms play a crucial role in amplifying the piezoelectric response, particularly in polycrystalline PZT ceramics. Understanding these extrinsic factors is essential for optimizing the piezoelectric performance of PZT-based materials for various applications. In technical applications of PZT films, achieving a substantial piezoelectric response requires careful consideration of these extrinsic effects, including domain reversal and movement.

Supporting Information: The process for preparing LaNiO_3 (LNO) conducting layer, SiO_2 buffer layer, and $\text{PbZr}_{0.53}\text{Ti}_{0.47}\text{O}_3$ films (PDF).

ACKNOWLEDGMENTS

We are immensely grateful to Associate Professor Naonori Sakamoto from the Faculty of Engineering at Shizuoka University for his technical support in acquiring transmission electron microscopy images.

V. REFERENCE

- ¹ Berlincourt, D.; Cmolik, C.; Jaffe, H. Piezoelectric properties of polycrystalline lead titanate zirconate compositions, Proc. IRE **1960**, *48*, 220-229. DOI: 10.1109/JRPROC.1960.287467.
- ² Jaffe, B.; Roth, R. S.; Marzullo, S. Piezoelectric properties of lead zirconate-lead titanate solid solution ceramics, J. Appl. Phys. **1954**, *25*, 809-810. DOI:10.1063/1.1721741.
- ³ Jaffe, B.; Cook, W. R.; Jaffe, H. *Piezoelectric Ceramics*, Academic: London, 1971.
- ⁴ Uchino, K. *Piezoelectric Actuators and Ultrasonic Motors*, Kluwer Academic Publishers: Boston, 1996.
- ⁵ Park, S.-E.; Shrout, T.E. Ultrahigh strain and piezoelectric behavior in relaxor based ferroelectric single crystals, J. Appl. Phys. **1997**, *82*, 1804-1811. DOI:10.1063/1.365983.
- ⁶ Saito, Y.; Takao, H.; Tani, T. ; Nonoyama, T.; Takatori, K.; Homma, T.; Nagaya, T.; Nakamura, M. Lead-free piezoceramics, Nature **2004**, *432*, 84-87. DOI:10.1038/nature03028.
- ⁷ Yang, S.; Bao, H.; Zhou, C.; Wang, Y.; Ren, X; Matsushita, Y; Katsuya, Y.; Tanaka, M.; Kobayashi, K.; Song, X.; Gao, J. Large magnetostriction from morphotropic phase boundary in ferromagnets, Phys. Rev. Lett. **2010**, *104*, 197201. DOI:10.1103/PhysRevLett.104.197201.
- ⁸ Bergstrom, R.; Wuttig, M.; Cullen, J.; Zavalij, P.; Briber, R.; Dennis, C.; Ovidiu Garlea, V.; Laver M. Morphotropic phase boundaries in ferromagnets: $Tb_{1-x}Dy_xFe_2$ Alloys, Phys. Rev. Lett. **2013**, *111*, 017203. DOI:10.1103/PhysRevLett.111.017203.
- ⁹ George, A. M.; Iniguez, J.; Bellaiche, L.; Effects of atomic short-range order on the properties of perovskite alloys in their morphotropic phase boundary, Phys. Rev. Lett. **2003**, *91*, 045504. DOI:10.1103/PhysRevLett.91.045504.
- ¹⁰ Fu, H.; Cohen, R. E. Polarization rotation mechanism for ultrahigh electromechanical response in single-crystal piezoelectrics, Nature **2000**, *403*, 281-283. DOI:10.1038/35002022.
- ¹¹ Guo, R.; Cross, L. E.; Park, S-E.; Noheda, B.; Cox, D. E.; Shirane, G. Origin of the high piezoelectric response in $PbZr_{1-x}Ti_xO_3$, Phys. Rev. Lett. **2000**, *84*, 5423-5426. DOI:10.1103/PhysRevLett.84.5423.
- ¹² Xu, G.; Wen, J.; Stock, C.; Gehring, P. M.; Phase instability induced by polar nanoregions in a relaxor ferroelectric system, Nature materials **2008**, *7*, 562-566. DOI:10.1038/nmat2196.

- ¹³ Noheda, B.; Cox, D.; Shirane, G.; Gonzalo, J.; Cross, L.; Park, S. A monoclinic ferroelectric phase in the $\text{Pb}(\text{Zr}_{1-x}\text{Ti}_x)\text{O}_3$ solid solution, *Appl. Phys. Lett.* **1999**, *74*, 13089. DOI: 10.1063/1.123756.
- ¹⁴ Noheda B.; Cox, D. E., Shirane, G.; Guo R.; Jones B.; L. E. Cross, L.E., Stability of the monoclinic phase in the ferroelectric perovskite $\text{PbZr}_{1-x}\text{Ti}_x\text{O}_3$, *Phys. Rev. B* **2000**, *63*, 014103. DOI: 10.1103/PhysRevB.63.014103.
- ¹⁵ Hall, D. A.; Steuwer, A.; Cherdhirunkorn, B.; Mori, T.; Withers P. J. A high energy synchrotron x-ray study of crystallographic texture and lattice strain in soft lead zirconate titanate ceramics *J. App. Phys.* **2004**, *96*, 4245-4252. DOI: 10.1063/1.1787590.
- ¹⁶ Hall, D. A.; Steuwer, A.; Cherdhirunkorn, B.; Mori, T.; Withers P. J. Analysis of elastic strain and crystallographic texture in poled rhombohedral PZT ceramics, *Acta Materialia* **2006**, *54*, 3075-3083. DOI: 10.1016/j.actamat.2006.02.043
- ¹⁷ Bassiri-Gharb, N; Fujii, I; Hong, E.; Trolier-McKinstry S.; Taylor, D. V.; Damjanovic D. Domain wall contributions to the properties of piezoelectric thin films, *J. Electroceram.* **2007**, *19*, 47-65: DOI:10.1007/s10832-007-9001.
- ¹⁸ Hinterstein, M.; Rouquette, J.; Haines, J.; Papet, Ph.; Knapp, M.; Glaum, J.; Fuess, H. Structural description of the macroscopic piezo- and ferroelectric properties of lead zirconate titanate, *Phys. Rev. Lett.* **2011**, *107*, 077602. DOI: 10.1103/PhysRevLett.107.077602.
- ¹⁹ Liu, H.; Chen, J.; Huang, H.; Fan, L.; Ren, Y.; Pan, Z.; Deng, J.; Chen, L-Q.; Xing, X. Role of reversible phase transformation for strong piezoelectric performance at the morphotropic phase boundary, *Phys. Rev. Lett.* **2018**, *120*, 055501. DOI: 10.1103/PhysRevLett.120.055501
- ²⁰ Fan, L.; Chen, J.; Ren Y.; Pan, Z.; Zhang, L.; Xing X. Unique piezoelectric properties of the monoclinic phase in $\text{Pb}(\text{Zr,Ti})\text{O}_3$ ceramics: large lattice strain and negligible domain switching, *Phys. Rev. Lett.* **2016**, *116*, 02760. DOI:10.1103/PhysRevLett.116.027601.
- ²¹ Fan, L.; Zhang, L.; Liu, H. Direct observation of polarization rotation in the monoclinic M_B phase under electrical loading, *Inorg. Chem.* **2021**, *60*, 15190-15195 . DOI:10.1021/acs.inorgchem.1c01599.
- ²² Wang, Z.; Zhang, N.; Yokota, H.; Glazer, A. M.; Yoneda, Y.; Ren, W.; Ye, Z-G. Local structures and temperature-driven polarization rotation in Zr-rich $\text{PbZr}_{1-x}\text{Ti}_x\text{O}_3$, *Appl. Phys. Lett.* **2018**, *113*, 012901. DOI:10.1063/1.5024422.
- ²³ Zhao, J.; Funni, S. D.; Molina, E. R.; Dickey, D. C.; Jones, J. L. Orientation-dependent, field-

- induced phase transitions in soft lead zirconate titanate piezoceramics, *J. Euro. Ceram. Soc.* **2021**, *41*, 3357-3362. DOI:10.1016/j.jeurceramsoc.2021.01.043.
- ²⁴ Sun, S.; Zhang, Y.; Fan, L.; Deng, S.; Gao, B.; Ren, Y.; Liu, H.; Chen, J. Role of tetragonal distortion on domain switching and lattice strain of piezoelectrics by in-situ synchrotron diffraction, *Scripta Materialia* **2021**, *194*, 113627. DOI:10.1016/j.scriptamat.2020.11.012.
- ²⁵ Li, J.; Rogan, R.; Ustundag, E.; Bhattacharya, K. Domain switching in polycrystalline ferroelectric ceramics. *Nature Mater* **2005**, *4*, 776-781. DOI:10.1038/nmat1485
- ²⁶ Asada, T; Koyama, Y. Ferroelectric domain structures around the morphotropic phase boundary of the piezoelectric material, *Phys. Rev. B*, **2007**, *75*, 214111. DOI: 10.1103/PhysRevB.75.214111.
- ²⁷ Otonicar, M.; Dragomir M.; Rojac, T. Dynamics of domain walls in ferroelectrics and relaxors, *J. Am. Ceram. Soc.* **2022**, *105*, 6479-6507. DOI: 10.1111/jace.18623.
- ²⁸ Gorfman, S.; Bokov, A. A.; Davtyan, A.; Reiser, M.; Xie, Y.; Ye, Z-G.; Zozulya, A. V.; Sprung, M.; Pietsch, U.; Gutt, C. Ferroelectric domain wall dynamics characterized with X-ray photon correlation spectroscopy, *PNAS*, **2018**, *115*, E6680-E6689. DOI:10.1073/pnas.1720991115.
- ²⁹ Shirane, G.; Suzuki, K. Crystal structure of $\text{Pb}(\text{Zr-Ti})\text{O}_3$, *J. Phys. Soc. Jpn.* **1952**, *7*, 333. DOI:10.1143/JPSJ.7.333.
- ³⁰ Clarke, R.; Whatmore, R. W.; Glazer, A. M. Growth and characterization of $\text{PbZr}_x\text{Ti}_{1-x}\text{O}_3$ single crystals, *Ferroelectrics*, **1976**, *13*, 497-500. DOI:10.1080/00150197608236650.
- ³¹ Phelan, D.; Long, X.; Xie, Y.; Ye, Z.-G.; Glazer, A. M.; Yokota, H.; Thomas, P. A.; Gehring, P. M. Single crystal study of competing rhombohedral and monoclinic order in lead zirconate titanate, *Phys. Rev. Lett.* **2010**, *105*, 207601. DOI: 10.1103/PhysRevLett.105.207601.
- ³² Bokov, A. A.; Long, X.; Ye, Z.-G. Optically isotropic and monoclinic ferroelectric phases in $\text{Pb}(\text{Zr}_{1-x}\text{Ti}_x)\text{O}_3$ (PZT) single crystals near morphotropic phase boundary, *Phys. Rev. B* **2010**, *81*, 172103. DOI:10.1103/PhysRevB.81.172103.
- ³³ Roleder, K.; Majchrowski, A.; Lazar, I.; Whatmore, R. W.; Glazer, A. M.; Kajewski, D.; Koperski, J.; Soszynski, A. Monoclinic domain populations and enhancement of piezoelectric properties in a PZT single crystal at the morphotropic phase boundary, *Phys. Rev. B* **2022**, *105*, 144104. DOI:10.1103/PhysRevB.105.144104.
- ³⁴ Lazar, I.; Whatmore, R. W.; Majchrowski, A.; Glazer, A. M.; Kajewski, D.; Koperski,

- J.; Soszynski, A.; Piecha, J.; Loska, B.; Roleder, K. Ultrahigh Piezoelectric Strains in $\text{PbZr}_{1-x}\text{Ti}_x\text{O}_3$ Single crystals with controlled Ti content close to the tricritical point, *Materials* **2022**, *15*, 6708. DOI:10.3390/ma15196708.
- ³⁵ Du, X.-H.; Zheng, J.; Belegundu, U.; Uchino, K. Crystal orientation dependence of piezoelectric properties of lead zirconate titanate near the morphotropic phase boundary, *Appl. Phys. Lett.* **1987**, *72*, 2421-2423. DOI:10.1063/1.121373.
- ³⁶ Saghi-Szabo, G.; Cohen, R. E.; Krakauer, H. First-principles study of piezoelectricity in tetragonal PbTiO_3 and $\text{PbZr}_{1/2}\text{Ti}_{1/2}\text{O}_3$, *Phys. Rev. B* **1999**, *83*, 12771-12776. DOI:10.1103/PhysRevB.59.12771.
- ³⁷ Bellaiche, L.; Vanderbilt, D. Intrinsic piezoelectric response in perovskite alloys: PMN-PT versus PZT, *Phys. Rev. Lett.* **1999**, *83*, 1347-1350. DOI:10.1103/PhysRevLett.83.1347.
- ³⁸ Bellaiche, L.; Garca, Al.; Vanderbilt, D. Finite-temperature properties of $\text{Pb}(\text{Zr}_{1-x}\text{Ti}_x)\text{O}_3$ alloys from first principles, *Phys. Rev. Lett.* **2000**, *84*, 5427-5430. DOI:10.1103/PhysRevLett.84.5427.
- ³⁹ Suzuki, H.; Miwa, Y.; Naoe, T.; Miyazaki, H.; Ota, T.; Fuji, M.; Takahashi, M. Orientation control and electrical properties of PZT/LNO capacitor through chemical solution deposition, *J. Euro. Ceram. Soc.* **2006**, *26*, 1953-1956. DOI:10.1016/j.jeurceramsoc.2005.09.037.
- ⁴⁰ Miyake, S.; Yamamoto, K.; Fujihara, S.; Kimura, T. (100)-orientation of pseudocubic perovskite-type LaNiO_3 thin films on glass substrates via the Sol-Gel process, *J. Am. Ceram. Soc.* **2002**, *85*, 992-994. DOI: 10.1111/j.1151-2916.2002.tb00206.x.
- ⁴¹ Schlom, D. G.; Chen, L.-Q.; Eom, C.-B.; Rabe, K. M.; Streiffer, S. K.; Triscone, J.-M. Strain tuning of ferroelectric thin films, *Annu. Rev. Mater. Res.* **2007**, *37*, 589-626. DOI: 10.1146/annurev.matsci.37.061206.113016.
- ⁴² Haun, M. J.; Furman, E.; Jang, S. J.; Cross, L. E. Thermodynamic theory of the lead zirconate-titanate solid solution system, part I: Phenomenology, *Ferroelectrics* **1989**, *99*, 13-25. DOI:10.1080/00150198908221436.
- ⁴³ Lee, H. J.; Shimizu, T.; Funakubo, H.; Imai, Y.; Sakata, O.; Hwang, S. H.; Kim, T. Y.; Yoon, C.; Dai, C.; Chen, L. Q.; Lee, S. Y.; Jo, J. Y. Electric-field-driven nanosecond ferroelastic-domain switching dynamics in epitaxial $\text{Pb}(\text{Zr,Ti})\text{O}_3$ film, *Phys. Rev. Lett.* **2019**, *123*, 217601. DOI:10.1103/PhysRevLett.123.217601.
- ⁴⁴ Grigoriev, A.; Sichel, R.; Lee, H. N.; Landahl, E. C.; Adams, B.; Dufresne, E. M.; Evans, P.G. Nonlinear piezoelectricity in epitaxial ferroelectrics at high electric fields, *Phys. Rev. Lett.*

- 2008**, *100*, 027604. DOI:10.1103/PhysRevLett.100.027604 .
- ⁴⁵ Fujisawa, T.; Ehara, Y.; Yasui, S.; Kamo, T.; Yamada, T.; Sakata, O.; Funakubo, H. Direct observation of intrinsic piezoelectricity of Pb(Zr,Ti)O₃ by time-resolved x-ray diffraction measurement using single-crystalline films, *Appl. Phys. Lett.* **2014**, *105*, 012905. DOI:10.1063/1.4889803.
- ⁴⁶ Li, Z.; Grimsditch, M.; Xu, X.; Chan, S.-K. The elastic, piezoelectric and dielectric constants of tetragonal PbTiO₃ single crystals, *Ferroelectrics* **1993**, *141*, 313-325. DOI: 10.1080/00150199308223459.
- ⁴⁷ Bellaiche, L.; Vanderbilt, D. Virtual crystal approximation revisited: application to dielectric and piezoelectric properties of perovskites, *Phys. Rev. B* **2000**, *61*, 7877-7882. DOI: 10.1103/PhysRevB.61.7877.
- ⁴⁸ Bellaiche, L. Piezoelectricity of ferroelectric perovskites from first principles, *Current Opinion in Solid State and Materials Science* **2002**, *6*, 19-25. DOI:10.1016/S1359-0286(02)00017-7.
- ⁴⁹ Ikegami, S.; Ueda, I.; Nagata, T. Electromechanical properties of PbTiO₃ ceramics containing La and Mn, *J. Acoust. Soc. Am.* **1971**, *50*, 1060-1066. DOI:10.1121/1.1912729.
- ⁵⁰ Damjanovic, D. Ferroelectric, dielectric and piezoelectric properties of ferroelectric thin films and ceramics, *Rep. Prog. Phys.* **1998**, *61*, 1267-1324. DOI:10.1088/0034-4885/61/9/002.
- ⁵¹ Hall, D.A. Review nonlinearity in piezoelectric ceramics. *J. Mater. Sci.* **2001**, *36*, 4575-4601 (2001). <https://doi.org/10.1023/A:1017959111402>

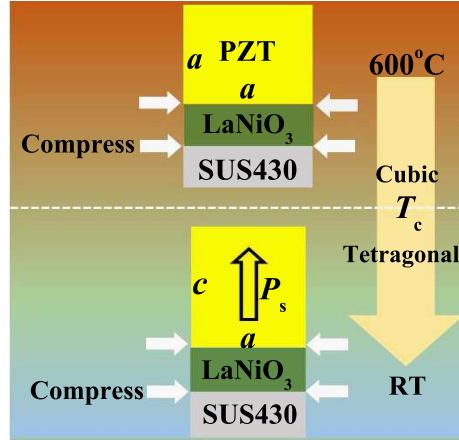


FIG. 1. Schematic diagram for growing c -axis oriented $\text{Pb}(\text{Zr}_{0.53}\text{Ti}_{0.47})\text{O}_3$ using compression from thermal stress.

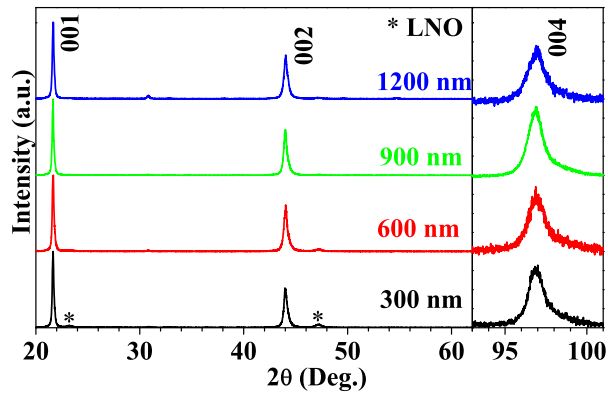


FIG. 2. X-ray diffraction patterns of c -axis oriented $\text{Pb}(\text{Zr}_{0.53}\text{Ti}_{0.47})\text{O}_3$ grown on a SUS430 substrate. * marks the diffraction peaks positions of LNO.

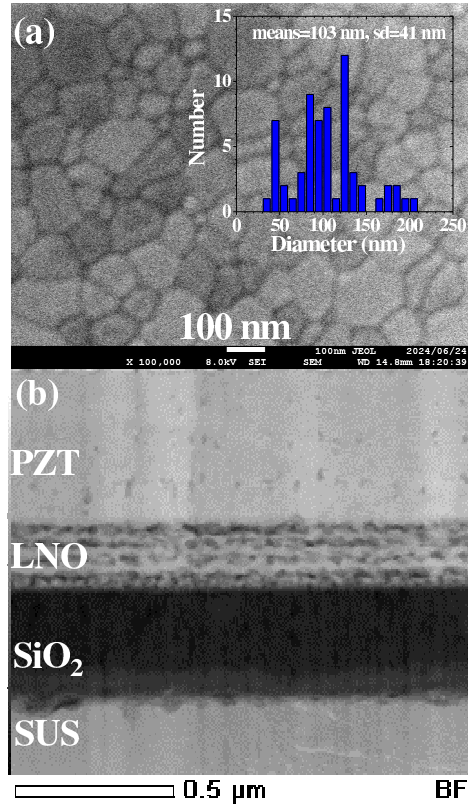


FIG. 3. (a) Surface and (b) cross-sectional images of c -axis oriented $\text{Pb}(\text{Zr}_{0.53}\text{Ti}_{0.47})\text{O}_3$ film. The distribution of the columnar PZT diameter is also shown in the inset of Figure (a).

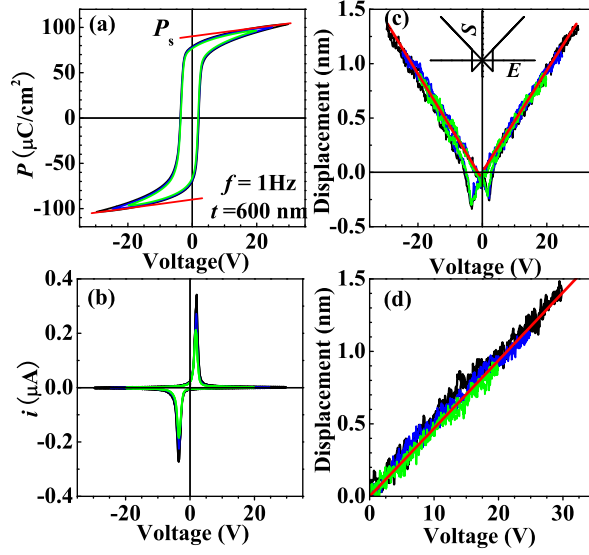


FIG. 4. (a) $D - E$ hysteresis loop, (b) the switching current and (c) the electric-field-induced displacements in c -axis oriented $\text{Pb}(\text{Zr}_{0.53}\text{Ti}_{0.47})\text{O}_3$ under bipolar voltage application. (d) Unipolar field-induced displacements. Inset in Fig.3(c) schematically shows an ideal strain-field response in a crystal, where spontaneous polarizations reverse only by 180° .⁵⁰

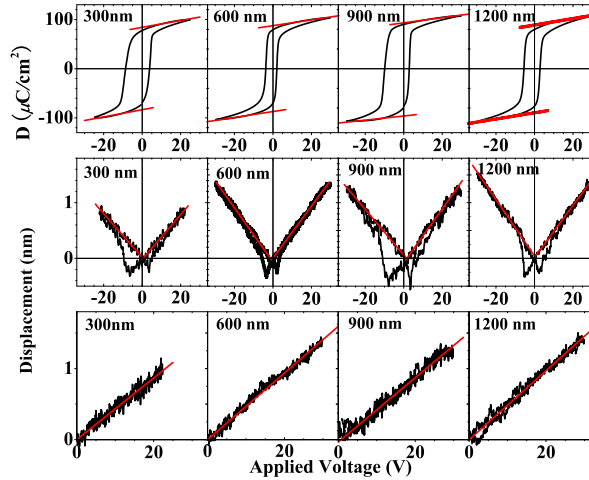


FIG. 5. $D - E$ hysteresis loop, bipolar and unipolar field-induced displacements in c -axis oriented $\text{Pb}(\text{Zr}_{0.53}\text{Ti}_{0.47})\text{O}_3$ films with thickness ranging from 300 nm to 1200 nm.

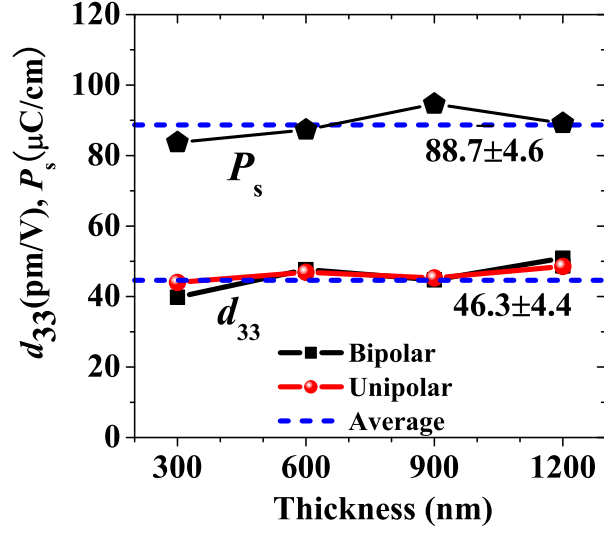


FIG. 6. The estimated d_{33} values and spontaneous polarization P_s for c -axis oriented $\text{Pb}(\text{Zr}_{0.53}\text{Ti}_{0.47})\text{O}_3$ films with thickness ranging from 300 nm to 1200 nm.

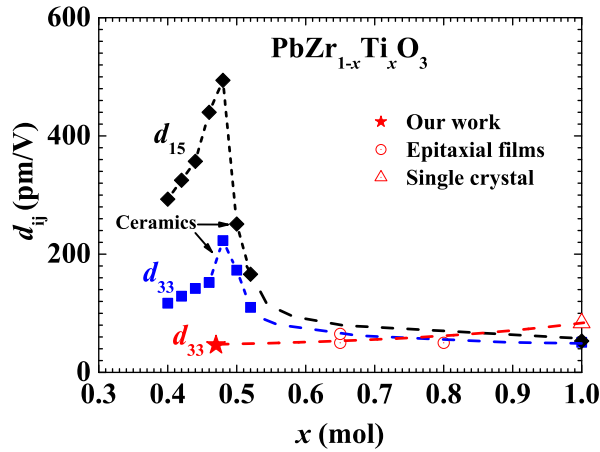


FIG. 7. Analysis of the piezoelectric coefficients of $\text{Pb}(\text{Zr}_{1-x}\text{Ti}_x)\text{O}_3$ ¹ and PbTiO_3 (PT)⁴⁹ ceramics in comparison to those of reported epitaxial PZT films^{43–45}, alongside the polar-axis-oriented $\text{Pb}(\text{Zr}_{0.53}\text{Ti}_{0.47})\text{O}_3$ films of this study and PT single crystal⁴⁶.